APPLIED SCIENCES AND ENGINEERING

Dynamic real-time imaging of living cell traction force by piezo-phototronic light nano-antenna array

Qiang Zheng[1†], Mingzeng Peng[1†], Zhuo Liu[1,2†], Shuyu Li[2], Rongcheng Han[3], Han Ouyang[1,2], Yubo Fan[2], Caofeng Pan[1,4], Weiguo Hu[1,4], Junyi Zhai[1,4]*, Zhou Li[1,4]*, Zhong Lin Wang[1,4,5]*

Dynamic mapping of the cell-generated force of cardiomyocytes will help provide an intrinsic understanding of the heart. However, a real-time, dynamic, and high-resolution mapping of the force distribution across a single living cell remains a challenge. Here, we established a force mapping method based on a "light nano-antenna" array with the use of piezo-phototronic effect. A spatial resolution of 800 nm and a temporal resolution of 333 ms have been demonstrated for force mapping. The dynamic mapping of cell force of live cardiomyocytes was directly derived by locating the antennas' positions and quantifying the light intensities of the piezo-phototronic light nano-antenna array. This study presents a rapid and ultrahigh-resolution methodology for the fundamental study of cardiomyocyte behavior at the cell or subcellular level. It can provide valuable information about disease detection, drug screening, and tissue engineering for heart-related studies.

INTRODUCTION

The heart is composed of billions of cardiomyocytes (*1*, *2*). The rhythmic, periodic, and disciplinary contraction of each cardiomyocyte enables the heart to pump blood efficiently at any moment. The cell-generated force of cardiomyocytes is crucial for understanding their activity, biomechanical properties, and state of health, which are closely related to their intrinsic biological processes (*3*–*5*), interaction between surrounded extracellular matrix or adjacent cells (*6*–*8*), and biochemical signal regulation (*9*, *10*). For quantifying the mechanical forces of cells, some techniques, such as traction force microscopy (*11*–*13*), optical tweezers (*14*, *15*), atomic force microscopy cantilevers (*16*, *17*), micropillar arrays (*18*–*20*), microelectro-mechanical system (MEMS) (*21*–*23*), and inserts and molecular sensors (*24*–*26*), have been adopted to elucidate and detect the cell traction force (CTF) (*27*), which is actively generated by the cell. However, these tools are either restricted for probing several scattered points on a cell surface or limited in the spatial resolution and temporal resolution, which are markedly important for kinetic cells such as cardiomyocytes. A fast, real-time, and high-resolution dynamic mapping of the force distribution across a cardiomyocyte during its beating cycle is vastly challenging.

In 2009, a vertically rigid silicon nanowire array–based method was used for quantifying the CTF of cancer and normal cells (*28*), which have increased the spatial resolution substantially to a record of 50,800 dots per inch (dpi). However, the lightproof substrate and the cell pretreatment of chemical fixation before surveying by scanning electron microscopy (SEM) in vacuum make this method incapable of observing live and dynamic cell behavior. By introducing photoluminescence (PL) materials (*29*, *30*), such as quantum dots, different vertically rigid nanowire arrays have been used for observing live cell movement. Fluorescence characterizes the location and shape of the cell and the magnitudes of the transverse displacements at the tips of nanowires. Nevertheless, it is difficult to directly derive and visualize an immediate value of CTF for real-time quantification.

The piezo-phototronic effect is a triple coupling effect composed of the piezoelectric effect, semiconductor properties, and photoexcitation in a piezoelectric semiconductor–based heterostructure. The key concept of the piezo-phototronic effect is using stain-generated piezoelectric polarization charges at the interface to modulate carrier generation, separation and transport, and/or recombination processes at the heterojunction (*31*, *32*). In this work, we designed and fabricated a uniform and well-aligned InGaN/GaN nanopillar array as a force-visualized detector, named piezo-phototronic light nano-antenna (PLNA) array, for CTF quantification. The PL of the multiple quantum wells (MQWs), which is at the tip of the InGaN/GaN nanopillar, is extremely sensitive to the inner piezo-potential. A tiny external force can change the intrinsic strain of the InGaN/GaN nanopillar, causing redistribution of the piezo-potential and then subsequently modulating the PL emission of the piezo-phototronic nanopillar. Therefore, the CTF of cardiomyocytes can be directly derived and visualized in both their resting and contraction states at an unprecedented spatial resolution of 800 nm and a temporal resolution of 333 ms, which shows the first image of CTF generated in the cell and the force-related dynamic process in different cycles. This method for measuring the mechanical behavior of live cardiomyocytes could be crucial for understanding the intrinsic process and behavior of cardiomyocytes and providing valuable information to guide the detection of biomechanically related diseases, the screening of drugs, and the evaluation of heart tissue engineering.

RESULTS

Schematic of measuring CTF by PLNA

As a dynamic cell force mapping method, the PLNA array is based on strain/piezo-potential tuned PL imaging. The basic working principle of the PLNA array is demonstrated in Fig. 1. The primary

[1]CAS Center for Excellence in Nanoscience, Beijing Key Laboratory of Micro-Nano Energy and Sensor, Beijing Institute of Nanoenergy and Nanosystems, Chinese Academy of Sciences, 100083 Beijing, China. [2]Beijing Advanced Innovation Center for Biomedical Engineering, Key Laboratory for Biomechanics and Mechanobiology of Ministry of Education, School of Biological Science and Medical Engineering, Beihang University, 100191 Beijing, China. [3]Institute of Genetics and Developmental Biology, Chinese Academy of Sciences, 100101 Beijing, China. [4]School of Nanoscience and Technology, University of Chinese Academy of Sciences, 100049 Beijing, China. [5]School of Materials Science and Engineering, Georgia Institute of Technology, Atlanta, GA 30332-0245, USA.
*Corresponding author. Email: jyzhai@binn.cas.cn (J.Z.); zli@binn.cas.cn (Z.L.); zhong.wang@mse.gatech.edu (Z.L.W.)
†These authors contributed equally to this work.

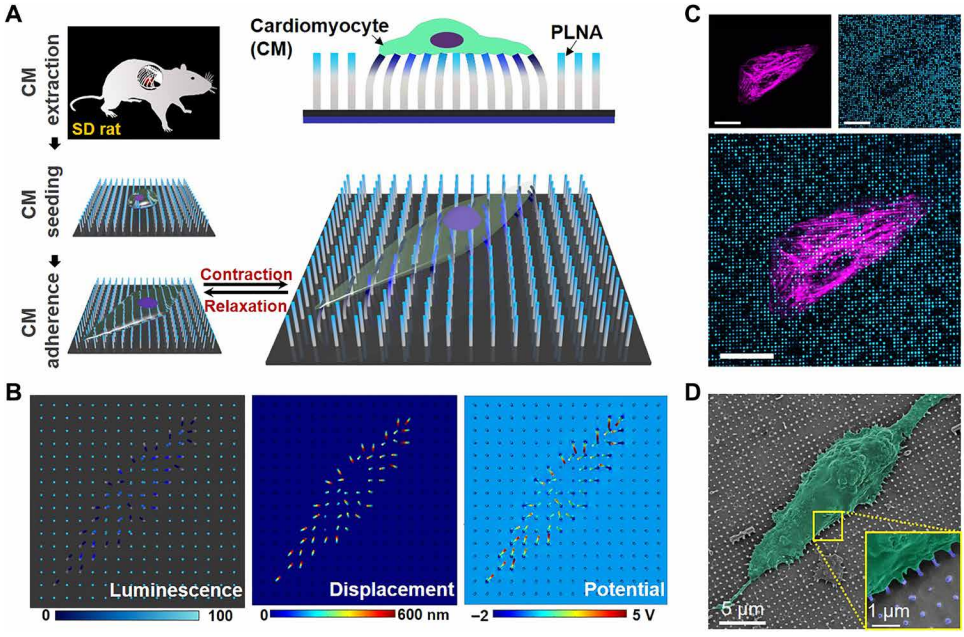

Fig. 1. Schematic of measuring CTF of a live cardiomyocyte by the PLNA arrayABCD. (**A**) Schematic diagram of the CTF detection process using the PLNA array. (**B**) Signal simulation of the strained PLNA array under CTF; from left to right: luminescence signal, displacement, and piezo-potential. (**C**) PL imaging of the cytoskeleton of a cardiomyocyte and its PLNA attached underneath: (top left: fluorescently stained cytoskeleton; top right: PL of the PLNA array; bottom: merged image; scale bars: 10 μm). (**D**) SEM image of an isolated cardiomyocyte and its PLNA attached underneath and partially enlarged detail, showing the bending of the nanopillars.

cardiomyocytes are extracted from neonatal Sprague-Dawley (SD) rats and seeded on the PLNA array (Fig. 1A). Before seeding cardiomyocytes, the PLNA array is modified with poly-L-lysine, which serves as an extracellular matrix to provide a suitable environment for the attachment and spreading of cardiomyocytes. By carefully controlling the cell seeding density and culture conditions, a single cardiomyocyte is beating on top of the device, which is crucial for mapping and analyzing CTF at the single-cell and subcellular level. The PLNAs underneath and the cell-bonded PLNAs are dragged by the cardiomyocyte to be bent transversely, resulting in a change of PL intensity. The intracellular molecular mechanism of measuring CTF by the PLNA array is shown in fig. S1.

The PLNA is made of an InGaN/GaN nanopillar with a diameter of 150 nm and an aspect ratio of 10:1. The PL can be generated at the InGaN/GaN MQW region (15 nm in thickness), which is at the tip of the nanopillar. Because of the piezo-phototronic effect (*33*), the PL of InGaN/GaN MQWs is ultrasensitive to mechanical stimulations, which can serve as the signal of PLNA. When an applied strain is induced to the InGaN/GaN nanopillar, piezoelectric charges will be generated at the interface between InGaN and GaN, which modulates the transport/separation/recombination of carriers at the MQW region. Thus, a tiny external force can tune the PL emission of the MQWs, especially the PL intensity (*31*, *32*). Once a cardiomyocyte is cultured on the PLNA array, the CTF will pull all cell-attached PLNAs and induce the change of regional PL intensity. The PLNA array serves as a function of high-density force sensor array for the distribution and the magnitude of the dynamic CTF in real time. The larger the CTF is, the higher the piezo-potential will be induced (Fig. 1B), which subsequently causes the larger change of PL intensity of the MQWs. The piezo modulation of the PL and the displacement of each PLNA are closely related to the CTF, which can be directly visualized and recorded by a confocal microscopy in real time.

In a living state, the contraction and relaxation of a cardiomyocyte will cause bending (strained) and the release (unstrained) of cell-attached PLNAs. The movement of the PLNAs results in position shifting of the lighting spots, which are from the MQWs at the free ends of PLNAs, and a change in the corresponding PL intensity, when under a fluorescence microscope. Therefore, PLNAs will present "shaking and switching" lighting nanospots of matrix, if there is a beating cardiomyocyte on its tip (Fig. 1C). The real-time PL intensity change rate ($\Delta I = (I_0 - I_s)/I_0$) from bright to dark in a cardiomyocyte beating cycle is the basic data for quantifying CTF, where I_δ and I_0 denote the PL intensity under the applied CTF at the contraction and relaxation state of cardiomyocyte, respectively, measured in situ by local confocal microscopy (Leica SP-8). On the basis of the data, we can quantitatively capture the real-time CTF either throughout the whole cell area or at a different region of a single contracting cardiomyocyte by using a charge-coupled device (CCD). In addition, the continuous and time-varying intensity change of PL, which takes place at about nanoseconds or even less, means that the PLNA array can meet the needs of recording a dynamic process at an ultrafast rate.

The mechanical force and resist compression in contracting cardiomyocytes are transmitted by the cytoskeleton, the distribution of which completely coincides with the CTF-induced shadow region in the PL image of the PLNA array of Fig 1C. A SEM image also demonstrates that the cell-attached PLNAs were obviously bent along the direction of cell contraction in Fig. 1D. All these results further indicate that the PLNA array can sensitively respond to the CTF in nanoscale spatial resolution.

Method of measuring CTF by the PLNA array

The PLNA array is fabricated by the state-of-the-art top-down approach from an epitaxial InGaN/GaN multilayer film grown on a

c-plane polished sapphire substrate, including a photolithography-patterned nickel metal dot matrix, low-damage dry etching of GaN-based thin films, and removal of the Ni metal mask (fig. S2). It shall be noted that no extra electrodes are needed here, which markedly reduces engineering complexity and extremely cuts down fabrication cost. As shown in Fig. 2A, the well-aligned and uniform PLNA array has a high pixel density of 31,750 dpi. Each PLNA is 150 nm in diameter and 1.5 μm in length. The center distance between two adjacent PLNAs is 800 nm (Fig. 2, B and C). Such vertically aligned ultrathin PLNA array can be fabricated in a large area with excellent uniformity in size, shape, period, and height. The large-area PLNA array is uniformly excited by a laser diode of 405 nm, showing a shiny blue fluorescent dot matrix, and its corresponding PL emission signal is at a peak wavelength of ~460 nm (fig S3). This device also shows great PL stability compared with traditional organic fluorescent dye. In a continuous 100-hour test under a cell culture environment, the PL intensity maintains extreme stability, showing great resistance against photobleaching, surface adsorption, and structural erosion (Fig. 2D). The high brightness, uniformity, and outstanding PL stability ensure a clearly defined and reproducible PL imaging for the force mapping.

Individual live cardiomyocytes are used to analyze the effect of dynamic CTF on the PLNA array that consists of InGaN/GaN MQWs. Although the bright-field imaging of a live primary cardiomyocyte is displayed on the PLNA array (Fig. 2E), the cell in the shadowed region can be observed to be clearly coincidental with the area where the fluorescence signal is changing (Fig. 2F). Using the ImageJ software, a calculated PL intensity image is shown in Fig. 2G,

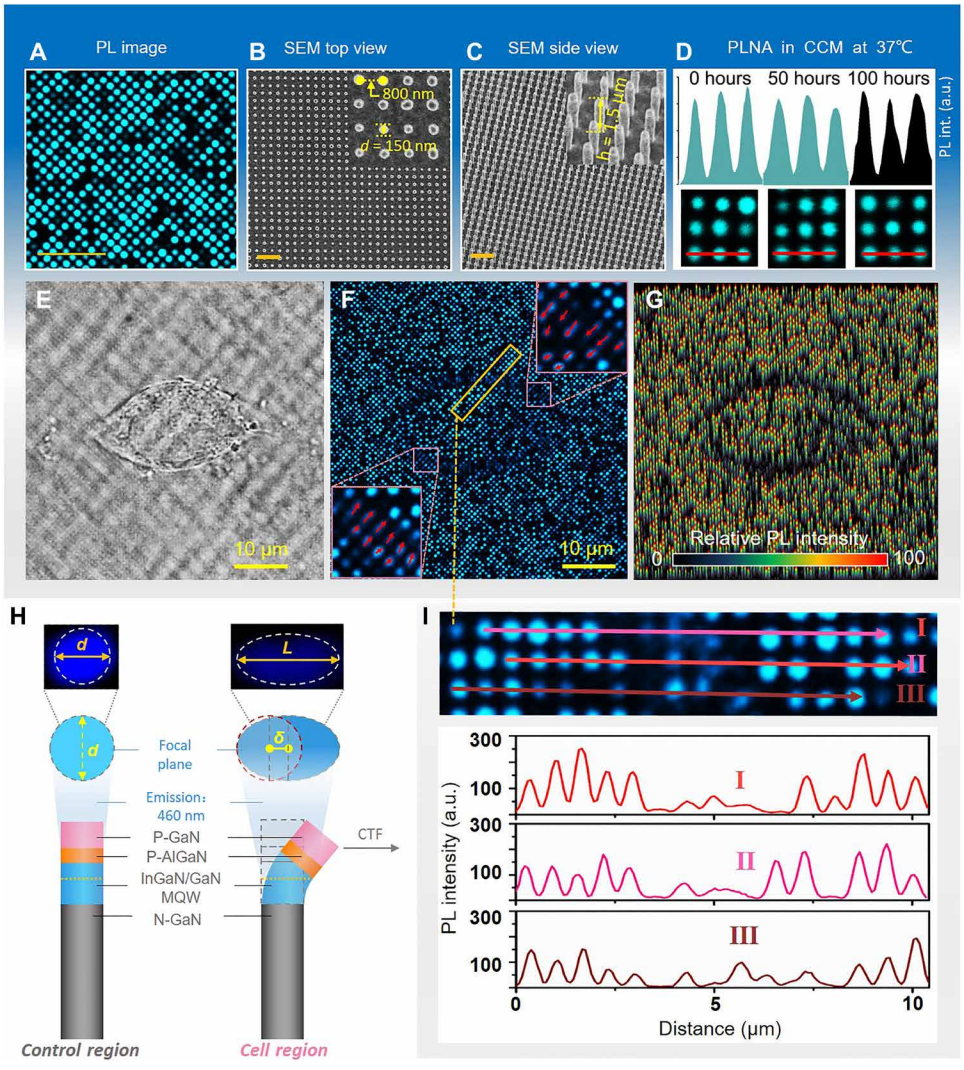

Fig. 2. Basic method for measuring the dynamic CTF in real time. (**A**) Fluorescent image of the as-fabricated PLNA array (scale bar, 2 μm). (**B** and **C**) SEM images of the as-fabricated PLNA array (scale bars, 2 μm). (**D**) PL stability of the PLNA array under 37°C in cell culture medium. a.u., arbitrary units. (**E**) Bright-field image of the tested live cardiomyocyte on the PLNA array. (**F** and **G**) PL image and its calculated PL intensity of the PLNA array. The represented "shadow" region was where a live cardiomyocyte located (inset: enlarged view of the selected region). (**H**) Basic model of the process for measuring the displacement of one PLNA under strain of CTF (left: the original state of one PLNA without the effect of CTF; right: the bending state of one PLNA under the CTF). (**I**) Real-time PL spectrum across the shadow region, revealing the PL intensity change of PLNAs under the CTF.

which clearly demonstrates the CTF-related fluorescence intensity distribution. The variation of PL intensity in the PLNA array can be directly read out by in situ local spectral measurement for the purpose of simultaneously quantifying CTF (Fig. 2I). With the increase of CTF, the change of PL intensity is more enhanced.

Besides quantifying CTF from PL intensity change, the displacement data of the PLNA array can be acquired through actual measurement of the position offsets of PLNAs from their initial positions by the software ImageJ. As shown in the insets of Fig. 2F, the light spots in the "shadow" region were obviously "elongated." We attributed this phenomenon to the CTF-induced bending of the PLNA and the consequent shift of its MQW region and the fluorescence projection onto the CCD of local confocal microscopy. The distance (δ) of the center point of the PLNA shifting from its original position after bending is measured as the displacement parameter of the PLNA under the CTF (Fig. 2H).

Real-time, dynamic CTF measurement of a beating cardiomyocyte by the PLNA array

Systematic studies are carried out to analyze the dynamic process of both fluorescence signal change and displacement variation of the PLNA array in a cardiomyocyte beat cycle. We trace the position information of 128 light spots in the range of tested cells frame by frame based on the continuous video image (movie S1). The displacement data of four randomly selected spots are plotted in Fig. 3A. They show an apparent periodicity of 900 ms, which is consistent with the beating rhythm that is observed in situ from bright-field video images of the same live cardiomyocyte (fig. S4). The maximum displacement was nearly 100 nm, corresponding to the maximum traction force at the cell contraction state.

The change in force/strain-sensitive PL intensity is a unique advantage of our method, which is ideal for dynamic visualization and quantification of CTF in living kinetic cells without a direct contact.

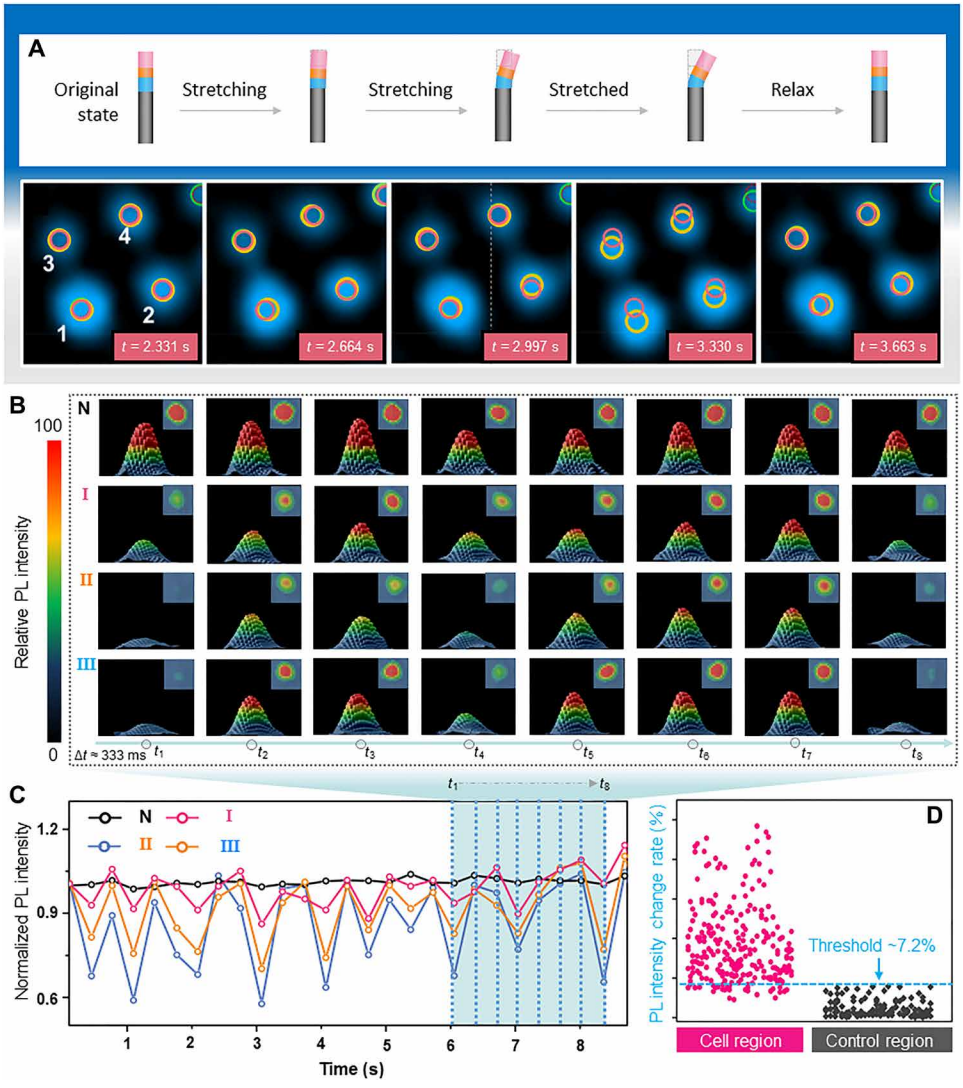

Fig. 3. Measurement of the displacement and the PL intensity change of PLNAs under the traction of a beating cardiomyocyte. (**A**) The PL images of four randomly selected PLNAs showing their displacements in a typical cardiomyocyte cycle (dashed red circle: the original position of PLNAs at the beginning of the cardiomyocyte cycle; yellow circle: the real-time position of PLNAs under cell traction). (**B** and **C**) Dynamic quantitative analysis of PL intensity change of four typical PLNAs. The PLNAs at the noncell region were selected as reference (N). (**D**) Standard deviations above the average PL intensity change rate for the cell region and the control region.

The shadow region of the PL image shares the same contour with the shape of the cell as provided by the bright-field optical image, which means that the fluorescent "off" state was mainly caused by the CTF after attaching the cell. Originating from the intrinsic traction force of the cardiomyocyte, a shear force was applied to each PLNA attached to the cell, which subsequently influenced its PL intensity owing to the piezo-phototronic effect of the MQW.

Time scale PL imaging is obtained for the real-time CTF information of cardiomyocytes (movie S2). We can obviously see alternating changes between bright and dark in the cell range as the cardiomyocyte rhythmically contracts and relaxes. Because the motion amplitude at different parts of a contracting cardiomyocyte is notably different, the maximum shear force applied to the related PLNAs is changed correspondingly. Therefore, the PL intensity change rate at different areas is also diverse. We selected four typical piezo-phototronic PLNAs in different regions for quantitative analysis. One (N) is located out of the cell region as a control group and the other three (I, II, and III) are located in the cell region. As shown in Fig. 3B, the PLNA of N presented a stable PL signal. The PL intensity of N remained almost the same throughout the testing period, while compared with the control group, the PL intensity of the other three PLNAs located in the cell region fluctuates significantly and periodically. The average cycle time is about 900 ms, which is also consistent with our measured contraction cycle of the cardiomyocyte. Taking PLNA II as an example, at the initial state of a contraction cycle, the brightness of the PLNA II is comparable with that of the control N. Once the cardiomyocyte begins to contract, the related fraction of the cell pulls this PLNA and results in a gradual darkening of its PL intensity until the end of contraction. After that, the cell begins to relax, and the PL intensity thus recovers to its initial state.

We also notice that the initial PL intensity is a little lower than that of the control N, which may derive from the interaction of two processes: (i) the slight scattering of light by the components of the cardiomyocyte and (ii) the tiny static strain on PLNAs caused by the slight weight of cell. The maximum PL intensity change rate can reach ~50% (II), and the intensity of the PLNA near the nucleus of the cardiomyocyte is only changed by 10% (I) (Fig. 3C). This difference characterizes the capability that our devices can reflect the tiny variation of CTF in different regions of a cell, which is significantly important for dynamic mapping of cell mechanics. The phenomenon of heterogeneity contraction, diminishing toward the nucleus of cardiomyocytes, is first described and quantified by dynamic CTF mapping. This advantage may give researchers more inspiration in fundamental research of cell mechanics, extracellular matrix, and reconstruction of cytoskeleton of cardiomyocytes and a new method for disease research and drug development.

Statistical analysis is carried out by measuring PL intensity change rate from numerous PLNAs located in and out of the region of contracting cardiomyocytes. The amplitude of PL intensity change rises markedly from the controlled region to the experimental region. Using a threshold of two standard deviations above the average PL intensity change rate of the controlled group, we found that more than 85% of experimental PLNAs showed obvious repeatable PL intensity change (Fig. 3D).

Further analysis can describe subregional (fig. S5) and whole-cell (fig. S6) mechanics at the real-time scale through PL imaging by fluorescence spectroscopy. Six regions of PLNAs under the cell are selected for further studies. They show quite clearly that the PL intensity and distribution in different regions are inhomogeneous. In the edge area of the cell, it appeared with a larger PL intensity fluctuation. In the area close to the internal part, the change of the PL intensity is smaller (fig. S5). This result reveals the inhomogeneous distribution of CTF across the whole cell, which is mainly due to the complex cell geometries, boundary conditions, and the natural inhomogeneous based on diversiform of materials, structures, and regional functions of a cell. The experiment of the PLNA response to CTF is shown in fig. S7, verified by the PL image of a live cardiomyocyte and the same cardiomyocyte exposed under ultraviolet (UV) for 15 min. In addition, the PLNA exhibits good biocompatibility, which indicates that the device can achieve long-term CTF detection (fig. S8).

Mechanism and modeling of the PLNA

There are three core parameters involved in CTF quantification: force, displacement, and PL (Fig. 4A). To realize the quantitative reading of CTF by measuring the PL intensity of PLNA, we need to establish the relevance between two parameters of the PL intensity variation ratio: spatial displacement and CTF. Figure 4B shows the relationship of the cell force (f_y) and the displacement of PLNA (d), which can be simply calculated by

$$f_y = \frac{3\pi E a^4}{2 l^3} d \tag{1}$$

where E is the Young's modulus (340 GPa) of the GaN, l is the length of the PLNA (1500 nm), and a is the radius of the PLNA (75 nm), respectively.

Figure 4 (C, original state, and D, stressed state) shows the mechanism of how the photoluminescence of InGaN/GaN MQW PLNAs is tuned by the external stress through the piezo-phototronic effect. Here, we chose one PLNA as the representative of the strain sensors. The z axis is set as the longitudinal direction of the PLNA as well as the c axis of the GaN, and the x axis is perpendicular to the z axis. The spontaneous polarization (polarization without external strain) of InGaN/GaN MQWs was only around −0.03 C/m^2, which was much smaller than the polarization constant of InGaN (0.97 C/m^2) and GaN (0.73 C/m^2). Thus, we could ignore the spontaneous polarization when we examined the tunability of photoluminescence of MQW through the external strain/stress-induced piezoelectric charges. As the original state, the PLNA was unstrained with the InGaN/GaN MQWs at the tip of the nanopillar. The quantum wells could be considered as flat due to the omission of the spontaneous polarization. In this case, photoluminescence processing has the maximum efficiency with the brightest luminescence spot. When the PLNA was bent (as shown in the left graph of Fig. 4D), the left-hand part of MQWs was elongated, while the right-hand part was contracted; thus, positive and negative piezoelectric charges were generated at the interfaces of the MQWs because of the asymmetric structure along the c axis of the wurtzite GaN and InGaN. Either positive or negative piezoelectric charges at the interfaces will make the quantum wells oblique, thus decreasing the photoluminescence efficiency of the MQWs and the intensity of the luminescence of the PLNA (*34*, *35*).

The photoluminescence intensity change rate can be derived from the change of the strain in the quantum wells due to the piezo-phototronic effect as (*35*, *36*)

$$\frac{I_s}{I_0} = \exp\left(-\frac{q e_{33} S_{33} W_{\text{piezo}}}{2\varepsilon_s \varepsilon_0 kT}\right) \tag{2}$$

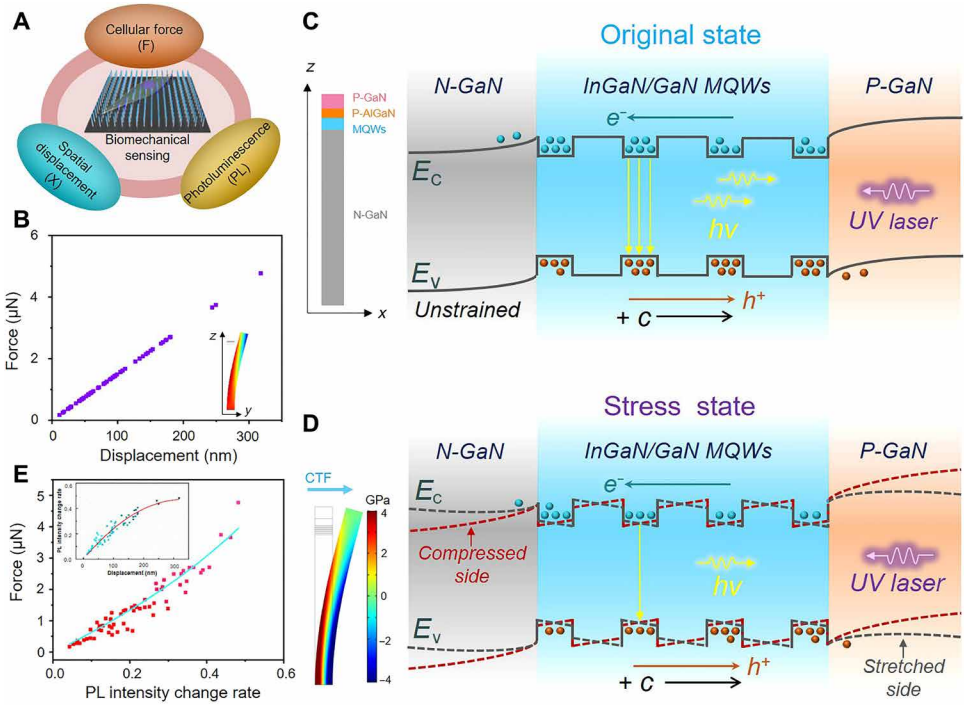

Fig. 4. Mechanism of CTF measurement based on the PLNA array. (**A**) Three core parameters involved in CTF monitoring. (**B**) Relationship of cell force and displacement of the PLNA. (**C** and **D**) Band diagram for understanding the PL change of the PLNA under cell traction. (**E**) Experimental (red dot) and fitting (violet line) results of the cell force upon the photoluminescence intensity change rate.

where I_s is the intensity of the PL under a certain strain, I_0 is the intensity of the PL without the external strain, q is the absolute value of unit electronic charge (1.6×10^{-19} C), e_{33} is the piezoelectric constant (0.73 C/m^2), ε is the relative dielectric constant (8.9), W_{piezo} is the piezoelectric depletion width (2.2 nm), T is the temperature (300 K), and k is the Boltzmann constant (1.38×10^{-23} J/K). Here, s_{33} is the absolute average stress along the longitudinal direction of the PLNA at the MQW position, which can be calculated by

$$s_{33} = \frac{2}{\pi a^2}\int_0^a \frac{8 f_y}{E\pi a^4} y\sqrt{a^2 - y^2}\,(l - z) \quad (3)$$

where y and z are the positions of the quantum well along the y and z axes, respectively. Figure 4E shows the experimental (dot) and fitting (line) results of the relationship between the PL intensity change rate and displacement distance, and the cell force upon the PL intensity change rate, which can be calculated as follows

$$\Delta I = \frac{I_0 - I_s}{I_0} = 1 - \exp\left(-\frac{4q\,e_{33}\,W_{piezo}(l - z)\,a}{\pi\varepsilon_s\varepsilon_0 kTl^3}d\right) \quad (4)$$

$$\Delta I = 1 - \exp\left(-\frac{8q\,e_{33}(l - z)\,W_{piezo}}{3\varepsilon_s\varepsilon_0 E\pi^2 a^3 kT}f_y\right) \quad (5)$$

where ΔI is the PL intensity change rate of the light spots, d is the displacement distance of the light spots, a is the radius of the nano-antenna (75 nm), l is the length of the nano-antenna (1500 nm), z is the distance from the MQW to the bottom of the nano-antenna (1340 nm), ε_0 is the vacuum dielectric constant (8.85×10^{-12} F/m), k is the Boltzmann constant (1.38×10^{-23} J/K), and T is the temperature (300 K), respectively .When the change of photoluminescence intensity is small, the force can be considered as a linear relationship with the change rate of photoluminescence intensity.

DISCUSSION

In this work, the PLNA array provides a new, unique, and quantitative method for directly "visualizing" CTF maps of a living cell in real time at an unprecedented time and spatial resolution. Table S1 shows a comparison of performance parameters related to the methods of measuring CTF by nano-/micro-pillar arrays (*19*, *28*, *37*–*39*). Instead of fixing and staining cells and manually measuring and calculating the CTF subsequently, the PLNA array permits to "image" and "read out" the distribution maps of single living cells in real time. Because there is a quantitative relationship between the strain/force-sensitive PL intensity change of PLNAs and the CTF, dynamic force change can be directly "imaged" by confocal microscopy in real time, without introducing any special cell treatment or equipment. The outstanding resolution (31,750 dpi) and pixel size (150 nm pixel^{-1}) facilitated an accurate measurement at many scales (whole-cell scale or subcellular scale). Therefore, the PLNA array is able to extract larger quantitative data and provide a more convincing analysis compared with older methods. The PLNA array exhibited amazing biocompatibility and stability. The newly extracted cardiomyocytes (one of the most difficult cells to cultivate) can easily survive for a long period onto the PLNA's surface. The dense PLNA array ensures that it will not adversely affect cell growth, crawling, and beating and creates a good growth environment similar to the normal culture conditions of cells. These results allowed us to study the true behavior and intrinsic state of many kinds of

cells. It is possible that the PLNA array has the potential to become a technology for phenotypic drug screening and discovery pertaining to conditions involving aberrant cellular force generation.

MATERIALS AND METHODS

Fabrication of the PLNA array

The PLNA was fabricated from an $In_{0.18}Ga_{0.82}N$/GaN MQW epitaxial multilayer thin film through a top-down semiconductor technique. The fabrication and the construction of the $In_{0.18}Ga_{0.82}N$/GaN MQW multilayer thin film were the same as previously described in (*33*). The top-down semiconductor technique includes the following processes: First, a highly ordered dot matrix was photolithography patterned by electron beam lithography, and the diameter and the period of nanopillars are 150 and 0.8 μm, respectively. Then, a pure Ni metal mask was deposited as the protective material through electron beam evaporation. Last, the PLNA was fabricated by an inductively coupled plasma etching technique. The length of each PLNA is 1.5 μm.

Characterization of the PLNA array

The nanostructure of PLNAs was carried out by SEM (SU8020). The high-resolution PL imaging measurement was based on a laser scanning confocal microscope (Leica SP8) and a spinning disk confocal microscope (ZEISS). According to the schematic diagram of the PL imaging measurement, we chose a semiconductor laser of 405 nm as the PL excitation source.

Primary culture of SD neonatal rat cardiomyocytes

SD neonatal rats were purchased from the Academy of Military Medical Sciences. The procedures in handling the animals were supervised by the Committee on Ethics of Beijing Institute of Nanogenerator and Nanosystems, which strictly conformed to the "Beijing Administration Rule of Laboratory Animal" and the national standards "Laboratory Animal Requirements of Environment and Housing Facilities (GB 14925–2001)." The hearts of SD rats were isolated via surgical operation and processed to separate and purify ventricular cardiomyocytes by mechanical trituration, collagenase II digestion (0.1%), filtration, and centrifugation. Nevertheless, the extracted cells might contain fibroblasts. To purify the cardiomyocytes, the method of differential adhesion was used. In brief, the cell suspension was inoculated on the culture dish; after 1 hour, the cell suspension was recycled. Because the adherent speed of the fibroblasts was faster than that of cardiomyocytes, 1 hour later, the filtration had adhered, but the cardiomyocytes had only just adhered. The recycled cell suspension was composed of purified cells. Trypan blue staining showed that 86.3% of extracted cells were positive.

The purified cardiomyocytes were cultured in Dulbecco's modified Eagle's medium (DMEM) (Hyclone) supplemented with 10% fetal bovine serum (FBS) (Gibco) and 1% penicillin-streptomycin solution (Macgene). Before inoculation, the PLNA array was sterilized by immersing it several times in 75% ethanol for 1 hour and under UV light for 30 min, and then the samples were washed three times for 5 min in sterile phosphate-buffered saline (PBS) to eliminate any residual ethanol.

The cardiomyocytes were seeded at a density of 1×10^5 cells/cm^2 on the PLNA array and incubated at 37°C in a humidified atmosphere with 5% CO_2. The culture medium was refreshed every 2 days.

Cardiomyocyte immunofluorescent staining

The cytoskeleton and nucleus were stained with phalloidin and 4′,6-diamidino-2-phenylindole (DAPI), respectively. In detail, the samples were fixed with immunohistochemically fixed fluid (Beyotime) for 30 min and then rinsed three times with prewarmed PBS. The samples were blocked with 0.1% bovine serum albumin solution for 1 hour at 37°C and then incubated with DAPI (1:400 diluted) and Alexa Fluor Phalloidin 568 conjugate (1:200 diluted) for 2 hours at 37°C. The DiI (Beyotime) was used to stain the live cardiomyocytes.

Cell compatibility of the PLNA

The material of the PLNA was immersed in DMEM with 10% FBS and 1% penicillin-streptomycin solution for 24 hours. This DMEM was used to culture the L929 cells as the experimental group. The L929 cells were seeded on 96-well plates with a density of 5000 cells per well. The MTT [3-(4,5-dimethylthiazol-2-yl)-2,5-diphenyltetrazolium bromide] assay was used to evaluate the proliferation of the cultured L929 cells, which can be taken up by living cells and reduced in the mitochondria to insoluble purple formazan granules. First, the MTT solution with 20 μl was added to each well. After incubating for 4 hours, the medium was discarded. Then, dimethyl sulfoxide with 100 μl per well was added to each well to dissolve the precipitated formazan. Last, the optical density of the solution was evaluated by a microplate spectrophotometer at a wavelength of 490 nm. MTT assay was performed at days 1, 2, and 3. At least four samples were randomly examined each time.

SUPPLEMENTARY MATERIALS

Supplementary material for this article is available at http://advances.sciencemag.org/cgi/content/full/7/22/eabe7738/DC1

REFERENCES AND NOTES

1. A. Foley, M. Mercola, Heart induction: Embryology to cardiomyocyte regeneration. *Trends Cardiovasc. Med.* **14**, 121–125 (2004).
2. A. P. Tendulkar, A. H. Harken, Mechanics of the normal heart. *J. Card. Surg.* **21**, 615–620 (2006).
3. L. Chen, V. Maybeck, A. Offenhäusser, H.-J. Krause, Characterization of the mechanical properties of HL-1 cardiomyocytes with high throughput magnetic tweezers. *Appl. Phys. Lett.* **107**, 053703 (2015).
4. J. G. Jacot, J. C. Martin, D. L. Hunt, Mechanobiology of cardiomyocyte development. *J. Biomech.* **43**, 93–98 (2010).
5. J. Wang, F. Lin, Z. Wan, X. Sun, Y. Lu, J. Huang, F. Wang, Y. Zeng, Y.-H. Chen, Y. Shi, W. Zheng, Z. Li, C. Xiong, W. Liu, Profiling the origin, dynamics, and function of traction force in B cell activation. *Sci. Signal.* **11**, eaai9192 (2018).
6. Y. Wang, E. L. Botvinick, Y. Zhao, M. W. Berns, S. Usami, R. Y. Tsien, S. Chien, Visualizing the mechanical activation of Src. *Nature* **434**, 1040–1045 (2005).
7. D. E. Discher, P. Janmey, Y.-l. Wang, Tissue cells feel and respond to the stiffness of their substrate. *Science* **310**, 1139–1143 (2005).
8. E. C. Butcher, E. L. Berg, E. J. Kunkel, Systems biology in drug discovery. *Nat. Biotechnol.* **22**, 1253–1259 (2004).
9. V. Vogel, Mechanotransduction involving multimodular proteins: Converting force into biochemical signals. *Annu. Rev. Biophys. Biomol. Struct.* **35**, 459–488 (2006).
10. W. H. Goldmann, Mechanical aspects of cell shape regulation and signaling. *Cell Biol. Int.* **26**, 313–317 (2002).
11. L. Qin, H. K. Genant, J. F. Griffith, K. S. Leung, *Advanced Bioimaging Technologies in Assessment of the Quality of Bone and Scaffold Materials: Techniques and Applications* (Springer Science & Business Media, 2007).
12. H. Colin-York, C. Eggeling, M. Fritzsche, Dissection of mechanical force in living cells by super-resolved traction force microscopy. *Nat. Protoc.* **12**, 783–796 (2017).
13. J. A. Mulligan, F. Bordeleau, C. A. Reinhart-King, S. G. Adie, in *Biomechanics in Oncology* (Springer, 2018), pp. 319–349.
14. H. Zhang, K.-K. Liu, Optical tweezers for single cells. *J. R. Soc. Interface* **5**, 671–690 (2008).
15. K. C. Neuman, A. Nagy, Single-molecule force spectroscopy: Optical tweezers, magnetic tweezers and atomic force microscopy. *Nat. Methods* **5**, 491–505 (2008).

16. W. A. Lam, O. Chaudhuri, A. Crow, K. D. Webster, T. D. Li, A. Kita, J. Huang, D. A. Fletcher, Mechanics and contraction dynamics of single platelets and implications for clot stiffening. *Nat. Mater.* **10**, 61–66 (2011).
17. A. V. Taubenberger, D. W. Hutmacher, D. J. Muller, Single-cell force spectroscopy, an emerging tool to quantify cell adhesion to biomaterials. *Tissue Eng. Part B Rev.* **20**, 40–55 (2014).
18. J. L. Tan, J. Tien, D. M. Pirone, D. S. Gray, K. Bhadriraju, C. S. Chen, Cells lying on a bed of microneedles: An approach to isolate mechanical force. *Proc. Natl. Acad. Sci. U.S.A.* **100**, 1484–1489 (2003).
19. O. du Roure, A. Saez, A. Buguin, R. H. Austin, P. Chavrier, P. Silberzan, B. Ladoux, Force mapping in epithelial cell migration. *Proc. Natl. Acad. Sci. U.S.A.* **102**, 2390–2395 (2005).
20. J. Fu, Y. K. Wang, M. T. Yang, R. A. Desai, X. Yu, Z. Liu, C. S. Chen, Mechanical regulation of cell function with geometrically modulated elastomeric substrates. *Nat. Methods* **7**, 733–736 (2010).
21. C. G. Galbraith, M. P. Sheetz, A micromachined device provides a new bend on fibroblast traction forces. *Proc. Natl. Acad. Sci. U.S.A.* **94**, 9114–9118 (1997).
22. J. Rajagopalan, M. T. A. Saif, MEMS sensors and microsystems for cell mechanobiology. *J. Micromech. Microeng.* **21**, 054002 (2011).
23. J. Rajagopalan, A. Tofangchi, M. T. A. Saif, Linear high-resolution bioMEMS force sensors with large measurement range. *J. Microelectromech. Syst.* **19**, 1380–1389 (2010).
24. O. Campàs, T. Mammoto, S. Hasso, R. A. Sperling, D. O'Connell, A. G. Bischof, R. Maas, D. A. Weitz, L. Mahadevan, D. E. Ingber, Quantifying cell-generated mechanical forces within living embryonic tissues. *Nat. Methods* **11**, 183–189 (2014).
25. C. Grashoff, B. D. Hoffman, M. D. Brenner, R. Zhou, M. Parsons, M. T. Yang, M. A. McLean, S. G. Sligar, C. S. Chen, T. Ha, M. A. Schwartz, Measuring mechanical tension across vinculin reveals regulation of focal adhesion dynamics. *Nature* **466**, 263–266 (2010).
26. X. Wang, T. Ha, Defining single molecular forces required to activate integrin and notch signaling. *Science* **340**, 991–994 (2013).
27. J. H.-C. Wang, J.-S. Lin, Cell traction force and measurement methods. *Biomech. Model. Mechanobiol.* **6**, 361–371 (2007).
28. Z. Li, J. Song, G. Mantini, M. Y. Lu, H. Fang, C. Falconi, L. J. Chen, Z. L. Wang, Quantifying the traction force of a single cell by aligned silicon nanowire array. *Nano Lett.* **9**, 3575–3580 (2009).
29. K. Adolfsson, H. Persson, J. Wallentin, S. Oredsson, L. Samuelson, J. O. Tegenfeldt, M. T. Borgström, C. N. Prinz, Fluorescent nanowire heterostructures as a versatile tool for biology applications. *Nano Lett.* **13**, 4728–4732 (2013).
30. M. Lard, H. Linke, C. N. Prinz, Biosensing using arrays of vertical semiconductor nanowires: Mechanosensing and biomarker detection. *Nanotechnology* **30**, 214003 (2019).
31. Z. L. Wang, J. Song, Piezoelectric nanogenerators based on zinc oxide nanowire arrays. *Science* **312**, 242–246 (2006).
32. Z. L. Wang, W. Wu, C. Falconi, Piezotronics and piezo-phototronics with third-generation semiconductors. *MRS Bull.* **43**, 922–927 (2018).
33. M. Peng, Z. Li, C. Liu, Q. Zheng, X. Shi, M. Song, Y. Zhang, S. du, J. Zhai, Z. L. Wang, High-resolution dynamic pressure sensor array based on piezo-phototronic effect tuned photoluminescence imaging. *ACS Nano* **9**, 3143–3150 (2015).
34. X. Huang, C. Jiang, C. du, L. Jing, M. Liu, W. Hu, Z. L. Wang, Enhanced luminescence performance of quantum wells by coupling piezo-phototronic with plasmonic effects. *ACS Nano* **10**, 11420–11427 (2016).
35. A. Zhang, M. Peng, M. Willatzen, J. Zhai, Z. L. Wang, Piezoelectric and deformation potential effects of strain-dependent luminescence in semiconductor quantum well structures. *Nano Res.* **10**, 134–144 (2017).
36. C. Pan, J. Zhai, Z. L. Wang, Piezotronics and piezo-phototronics of third generation semiconductor nanowires. *Chem. Rev.* **119**, 9303–9359 (2019).
37. D. B. Suyatin, W. Hallstrom, L. Samuelson, L. Montelius, C. N. Prinz, M. Kanje, Gallium phosphide nanowire arrays and their possible application in cellular force investigations. *J. Vacuum Sci. Technol. B Microelectron. Nanometer Struct. Process. Measure. Phenom.* **27**, 3092–3094 (2009).
38. S. Ghassemi, G. Meacci, S. Liu, A. A. Gondarenko, A. Mathur, P. Roca-Cusachs, M. P. Sheetz, J. Hone, Cells test substrate rigidity by local contractions on submicrometer pillars. *Proc. Natl. Acad. Sci. U.S.A.* **109**, 5328–5333 (2012).
39. J.-Y. Shiu, L. Aires, Z. Lin, V. Vogel, Nanopillar force measurements reveal actin-cap-mediated YAP mechanotransduction. *Nat. Cell Biol.* **20**, 262–271 (2018).

Acknowledgments: We thank Y. Zhang (BUAA), Y. Jin (BINN), X. Qu (BINN), and K. Yu (BUAA) for discussion and experimental and technical support. We are grateful to all the laboratory members for their cooperation in this study. **Funding:** This study was supported by the National Natural Science Foundation of China (nos. 61875015, 51872031, and 82001982), the Beijing Natural Science Foundation (JQ20038 and 7204333), the China Postdoctoral Science Foundation (2020M680302 and 2019M660410), the Fundamental Research Funds for the Central Universities, and the National Youth Talent Support Program. **Author contributions:** Z.L.W., Z. Li, and J.Z. conceived the idea and guided the project. Q.Z., Z. Liu, M.P., Z. Li, and J.Z. designed the experiment. Z. Li, J.Z., and M.P. designed and fabricated the PLNA. Z. Liu, Q.Z., and M.P. characterized the morphology and structure of the PLNA. Z. Liu carried out cell experiments. Z. Liu, Q.Z., and R.H. performed the cell observation. Y.F., H.O., and S.L. carried out the COMSOL simulation and MATLAB analysis. Y.F., C.P., and W.H. participated in the data discussion. Q.Z., Z. Liu, Z. Li, and J.Z. analyzed the data and prepared the figures. Q.Z., Z. Liu, Z. Li, J.Z., and Z.L.W. wrote and revised the manuscript. **Competing interests:** The authors declare that they have no competing interests. **Data and materials availability:** All data needed to evaluate the conclusions in the paper are present in the paper and/or the Supplementary Materials. Additional data related to this paper may be requested from the authors.

Submitted 14 September 2020
Accepted 8 April 2021
Published 26 May 2021
10.1126/sciadv.abe7738

Citation: Q. Zheng, M. Peng, Z. Liu, S. Li, R. Han, H. Ouyang, Y. Fan, C. Pan, W. Hu, J. Zhai, Z. Li, Z. L. Wang, Dynamic real-time imaging of living cell traction force by piezo-phototronic light nano-antenna array. *Sci. Adv.* **7**, eabe7738 (2021).